Journal of Water Process Engineering 48 (2022) 102816

Contents lists available at ScienceDirect

Journal of Water Process Engineering

journal homepage: www.elsevier.com/locate/jwpe

Optimum recovery of saline gradient power using reversal electrodialysis: Influence of the stack components

L. Gómez-Coma, J.A. Abarca, M. Fallanza, A. Ortiz, R. Ibáñez, I. Ortiz *

Department of Chemical and Biomolecular Engineering, Universidad de Cantabria, Av. Los Castros 46, 39005 Santander, Spain

ARTICLE INFO

Keywords:
Salinity gradient power (SGP)
RED technology
Gross power density
Water sustainability

ABSTRACT

Salinity gradient power (SGP), has gained attention in last years, due to its numerous advantages as renewable and continuous source of energy. Furthermore, the possibility of deploying this new source of green energy in coastal wastewater treatment plants (WWTPs) offers an attractive alternative to advance the energy sustainability in these installations while contributing to increase the prospects for water reclamation. As part of a global project that integrates the recovery of SGP through reverse electrodialysis within a water reclamation process, we report the analysis of the influence of the main components of a reversal electrodialysis (RED) stack, membranes, and spacers, on the recovery of energy. Additionally, the optimal number of cell pairs and velocity of the water streams is determined to maximize the gross power density. The study is carried out with model waters with a sodium chloride concentration of 0.5 M (seawater) and 0.02 M (close to WWTP effluents) as high and low concentration solutions respectively, in a RED stack with 3 to 20 ion exchange membrane pairs. The results reveal that membrane thickness exerts a more decisive influence than the spacers thickness. Power density values as high as 1.59 W·m^{-2} and 1.77 W·m^{-2} have been obtained using membranes of 50 μm thickness and spacers of 270 and 155 μm thickness, respectively. The information here reported helps in the decision-making for the proper design of the membrane stack, making a step forward to facilitate the integration of SGP recovery within water reclamation processes, reducing fossil fuel dependence in WWTPs.

1. Introduction

The 2030 Agenda for Sustainable Development, adopted by all United Nations Member States, provides different objectives to achieve a better and more sustainable future for all people [1]. In this sense, 17 sustainable development goals (SDG) have been stablished focusing on diverse interconnected areas. Specifically, ODS number 7 called "Affordable and Clean Energy" and ODS number 9 "Climate Action" are closely linked, and encouraging the progress of new green energy sources that are competitive with fossil fuel-based energy sources. Besides, the ODS number 6 "*Clean Water and Sanitation*" seeks to promote accessible and sustainable management of water for all.

In this context, salinity-gradient power (SGP) or Blue Energy has emerged as one of the most promising sources of renewable energy in the 21st century for medium and large-scale applications. Theoretically, SGP allows generating, according to the Gibbs free energy, up to 1.7 MJ by mixing 1 m^3 of seawater with the same amount of river water [2]. This type of energy is based on the salinity difference between two water streams, known as high concentration (HC) and low concentration (LC) streams, respectively. In the first case, seawater, saline water bodies or brines are commonly used as HC streams, while river water, wastewater effluents or water wells represent typical examples of LC streams. In the case of wastewater treatment plants (WWTPs), previous works demonstrated the possibility of reducing the energy consumption of these facilities and reducing the water stress through the development of tertiary processes that integrate water reclamation units and energy recovery through the reverse electrodialysis technology; the final LC water with a slight increase in its salinity after the RED unit would serve to different uses such as sanitation, street cleaning or even irrigation [3–5]. Besides, other important features of the salinity gradient power are the continuous production of energy, in contrast to the intermittency of solar or wind energy, and the fact that wastes are not produced.

In addition to Reverse Electrodialysis (RED) that is based on the use of ion-exchange membranes (IEM) [6,7], Pressure Retarded Osmosis (PRO) [8–13] and capacitive deionization [14] have been proposed as feasible technologies to harvest SGP. PRO and RED technologies are relatively close to the state of commercialization, however, remaining issues, such as membrane lifetime, mainly limited by fouling

* Corresponding author.
E-mail address: ortizi@unican.es (I. Ortiz).

https://doi.org/10.1016/j.jwpe.2022.102816
Received 13 March 2022; Received in revised form 18 April 2022; Accepted 21 April 2022
Available online 8 May 2022

phenomenon, and membrane high cost, continue to be the major drawbacks for their widespread deployment. PRO technology, conceptualized by Prof. Loeb in 1974 [15], harvests energy by using semi-permeable membranes allowing the transport of water from the LC to the HC solution under the influence of a pressure difference [7]. Apart from membrane fouling an additional drawback of this alternative is the high amount of energy consumed in the process by a pressure exchanger, which decreases the available net power [12]. RED technology, firstly developed in 1954 by R.E. Pattle [16], avoids this problem. In this case, salt ions are transferred from the HC to LC streams through the IEMs due to the concentration difference [17]. The elementary unit of a RED stack is the cell pair, composed of a cation exchange membrane (CEM), a dilute compartment, and an anion exchange membrane. Typically, RED systems use standard-grade membranes [5,17–22], ideally with very low resistance, high selectivity and high stability in acidic and basic conditions. Besides, new types of IEMs for RED stacks are currently being developed, such as, i) a new generation of monovalent membranes, ii) novel multivalent permeable membranes with antifouling properties, and iii) profile membranes. Monovalent membranes are of special interest since they allow the facilitated transport of single charge ions while blocking the crossover of multivalent ions [23–26]. This type of membranes can be fabricated by surface layer modification or by the formation of highly cross-linked materials [25–27]. Preventing uphill phenomena, that is the undesired transport of multivalent ions from the LC solution to the HC solution, is the main advantage of monovalent membranes [28,29]. Nevertheless, some recent works reported high values of membrane resistances for monovalent membranes and, consequently, poor RED performance [29–31]. Thus, when ion-selective membranes are used, a trade-off between the enhancement of monovalent ions selectivity and membrane resistance must be considered [25]. In contrast, multi-permeable membranes are well-known and cheaper than monovalent membranes and are frequently used for long-term experiments [4,5,32,33]. In fact, two pilot plants have been constructed using RED systems and, in both cases, they employ multivalent membranes. The first one, located in Marsala (Italy), was based on the contact between brines and brackish water as HC and LC respectively and the second one, in Afsluitdijk (The Netherlands), flows seawater and river water [18,33]. Laboratory scale studies using nonselective or multivalent IEMs currently focus on the prevention of fouling caused by non-single charged ions, which negatively increases membrane resistance and consequently reduces the RED performance [4,22,28–35]. However, recent studies highlight that a simple tertiary treatment, entailing, coagulation, flocculation, decantation, and filtration could significantly reduce membrane fouling [5]. Other water sources such as the rejection of reverse osmosis units in desalination plants also offer the potential for water reclamation and do not require additional treatment. In this framework, Mei et al. published an interesting work highlighting the technical feasibility and the current practical constraints of the RED technology combined with electrodialysis to contribute to self-sufficient desalination plants. The work mentioned above sets the basis to achieve a salt removal efficiency and a freshwater recovery through more energy-efficient desalination methods [36].

Finally, profiled membranes or spacerless membranes include a relief on their surface that substitutes the role of spacers and leads to low ohmic resistance values due to their ion-conducting structures with low hydraulic friction, but the boundary layer resistance is higher revealing poor promotion of mixing [37–40]. As Mei and Tang reported, these membranes are designed with tailored microstructures such as ridges, waves, pillars, or chevron corrugation, to conduct water streams [40]. Some works have studied the performance of profiled membranes to extract blue energy; for example, Vermaas et al. pointed out that profiled membranes are significantly less sensitive to fouling and are easier to be cleaned than stacks with spacers [33]. Nazif et al. highlighted that the use of this type of membranes avoids the spacer shadow effect, where a large portion of the conductive membrane area is covered with the spacers, providing higher membrane area [41]. In addition, other works revealed the reduction of pumping energy when profiled membranes are assembled in substitution of traditional membranes-spacers configurations [40,42]. However, the spacer substitution can promote the formation of dead zones and polarization phenomena [40,42,43]. Another critical disadvantage of these membranes consists in keeping the characteristics of the membranes when they are removed from the moulds [33,43]. Thus, despite profiled membranes holding promise to improve RED performance, this option still offers high complexity, and therefore further research is required to reach the market.

Nowadays, the use of a spacer mesh to separate the IEMs is mostly adopted to improve the contact of the solutions as well as to enhance flowrate distribution of water streams along the membrane compartments [2,5,17–20,44,45]. In this sense, in RED technology, spacers also play an important role to keep the convenient distance between membranes [44] Thus, the membrane properties and intermembrane distance have a significant impact on the overall process performance. One of the key features of spacers with influence on RED performance is the mesh porosity. Generally, lower porosity values imply higher compartment resistance [17,44]. In addition, small intermembrane distance (spacer thickness) favors the reduction of the stack resistance but, simultaneously, limits the water stream flow rates and increases the pressure drop [20]. Then, the configuration of spacers is critical and plays an important role in RED efficiency that needs to be exhaustively examined and optimized.

WWTPs are high energy consumers, 0.5 $kWh \cdot m^{-3}$, with a strong dependence on fossil fuels. Therefore, previous works analyzed low concentration stream and seawater as HC solutions to maximize the energy recovery when employing RED technology and consequently improve WWTPs sustainability. These works concluded that 0.02 M in terms of salinity is the optimal value which is close or slightly lower (a value that can be easily increased) than the typical salinity of WWTPs secondary effluents. Therefore, the installation of SGP appears to be a promising strategy to facilitate energy recovery when integrated with water reclamation strategies; this alternative, more attractive to WWTPs located in coastal areas, would decrease water stress and reduce the use of fossil fuels. [5,46].

However, it is essential to remark that despite the high expectations raised, further research efforts are necessary so that the technological alternatives to the recovery of SGP become commercially available [46,47]. In this way, this work aims to analyze the influence of the key components in a RED stack, more specifically the thickness of both spacers and monovalent-membranes as well as membrane pairs and linear velocity of the aqueous streams flowing through the RED stack. Thus, the gained knowledge will facilitate the development of this promising green source of energy and, at the same time, will potentiate its integration in water reclamation processes.

2. Experimental

Two different multivalent commercial types of cationic (FKS-50 and FKS-30) and anionic (FAS-50 and FA-30) exchange membranes have been used and supplied by Fumasep® (Germany). The membrane

Table 1
Cationic (CEM) and anionic (AEM) exchange membrane characteristics according to Fumasep®.

Membrane	Thickness (μm)	Permselectivity 0.1–0.5 M (%)	Area resistance ($\Omega \cdot cm^2$)
FAS-50 (AEM)	45–55	92–96	0.6–1.5
FAS-30 (AEM)	25–35	92–96	0.3–0.6
FKS-50 (CEM)	45–55	97–99	1.8–2.5
FKS-30 (CEM)	21–26	99	0.84

effective area was 200 cm^2, and the main membrane properties in terms of thickness, permselectivity and area resistance are summarized in Table 1. Membranes were assembled in a RED stack provided by Fumatech® (Germany). Polyethersulfone spacers, 155 μm and 270 μm thickness and with a porosity of 82.5% were placed between membranes.

A solution composed of 0.05 M $K_3Fe(CN)_6$, 0.05 M $K_4Fe(CN)_6$, and 0.25 M NaCl in deionized water was employed as electrolyte [48]. Eq. 1 shows the redox reaction; the electrolyte, which converts the ionic current into an electrical current, is continuously recirculated. At the end of the RED stack two electrodes integrated mainly by titanium/mixed oxides were placed and prevent the loss of the iron complex. CEM outer membranes were placed at both sides of the RED stack to ensure the circuit closure [49].

$$\left[Fe(CN)_6\right]^{3-} + e^- \leftrightarrow \left[Fe(CN)_6\right]^{4-} \tag{1}$$

The experiments were carried out with solutions of sodium chloride (NaCl) (assay > 99.5, Fisher Chemicals). In this sense, NaCl 0.5 M salinity, was prepared and used as high concentration solution. On the other hand, 0.02 M NaCl solution was employed as a low concentration solution, since it was previously reported that it favors the optimal SGP-RED performance [46].

The configuration of the experimental setup has been detailed in previous works [17,46] and is briefly depicted in Fig. 1. In summary, both streams feed the RED module in parallel entering the bottom part of the stack and leaving it, without mixing, from the top. The experiments were performed using an electronic load in galvanostatic mode (Chroma Systems Solutions 63103A, USA) and the electrical current was modified measuring the produced voltage. The value of the current was maintained until reaching constant voltage and every experiment was replicated at least three times as independent tests. Moreover, the experimental setup was introduced in an oven to guarantee isothermal conditions (24 °C) due to the strong influence of temperature on the technology performance [17].

3. Results and discussion

This section presents the main results obtained when different membranes and spacers were tested in a module for the recovery of SGP. Moreover, since a parasitic resistance (from the high potential to the low potential electrode compartment) was previously observed, which could present high impact on the RED performance, in this work, the influence of the number of cell pairs has also been studied [11,50]. The performance has been evaluated in terms of the gross power density per membrane pair ($W{\cdot}m^{-2}$) versus the current intensity. Finally, the influence of the linear velocity, increasing from 1 to 3 $cm{\cdot}s^{-1}$, was studied with the different spacers and membranes. Using RED technology, when tertiary wastewaters are used as low concentration feed, the outlet water fulfills the allowable concentration in the target parameters such as turbidity, total suspended solids, or conductivity for reuse in urban activities like street cleaning and fire systems, industrial applications, or irrigation [5].

Besides, for the ease of reading, all the experiments carried out with 155 μm are referred to with a triangle (▲) while 270 μm spacers are represented with a circle (●). When 3 membrane pairs were used, purple colour was chosen to represent the points while 5, 10, 15, and 20 cell pairs were characterized with blue, orange, red, and green colors, respectively. Finally, ion exchange membranes of 30 μm are showed with filled symbols ▲ or ● and 50 μm with unfilled symbols △ or ○. Table 2 summarizes the legends used in this paper in terms of symbols and colors.

3.1. Influence of the spacers thickness

This section discusses the influence of the spacers in the recovery of SGP using the reversal electrodialysis technology. In this sense, different experiments have been developed using both spacers with 155 and 270 μm and 30 μm membrane thickness. In this case, the linear velocity was 2.5 $cm{\cdot}s^{-1}$. Fig. 2 shows the power curves generated when different cell pairs were installed. Fig. 2 also depicts that both variables, power density and current intensity, are higher for the same number of membrane pairs when 155 μm spacers were employed. In this sense, when 20 cell pairs were installed, the power density achieved constant values: 1.4 $W{\cdot}m^{-2}$, and 1.2 $W{\cdot}m^{-2}$ and the limiting current, 0.75 A and 0.9 A for the spacers thickness of 155 μm and 270 μm, respectively. These values are in concordance with previous works reported in literature using seawater as a high concentration stream [51–53]. These results are justified since the distance between the membranes in a membrane pair is a key parameter in the total stack resistance determined as the sum of the ohmic and non-ohmic parts [53]. In particular, the ohmic resistance is determined by the membrane resistances (R_{AEM} and R_{CEM}) and the compartment resistances (R_{HC} and R_{LC}) of the high and low

Table 2
Summary of the legend used in the Figures reported in this work.

Spacer thickness	Membranes	Number of cell pairs	
			3
155 μm	30 μm ▲		5
	50 μm △		10
270 μm	30 μm ●		15
	50 μm ○		20

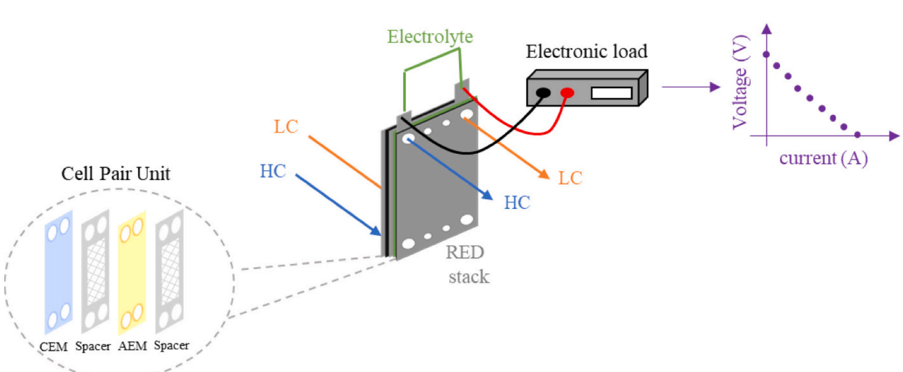

Fig. 1. Brief scheme of the experimental set-up.

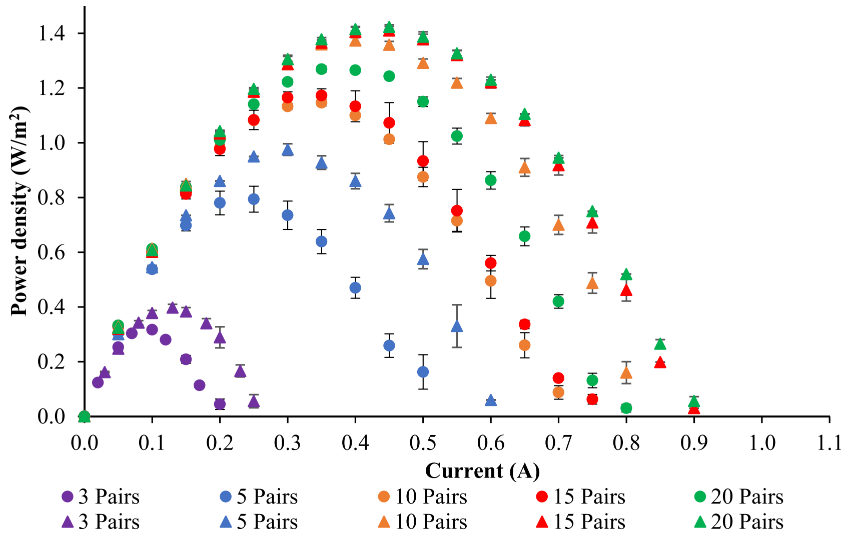

Fig. 2. Spacer thickness influence. Membrane thickness = 30 μm, linear velocity = 2.5 cm·s^{-1}. ● = 270 μm spacers. ▲ = 155 μm spacers.

concentration streams. Eqs. 2a and 2b detail the simplified expression of the ohmic resistance, and the different contributions to R_{HC} and R_{LC}, respectively.

$$R_{ohmic} = R_{AEM} + R_{CEM} + R_{HC} + R_{LC} \tag{2a}$$

$$R_{ohmic} = R_{AEM} + R_{CEM} + \frac{\delta}{\varepsilon^2 \cdot conduct_{HC}} + \frac{\delta}{\varepsilon^2 \cdot conduct_{LC}} \tag{2b}$$

where δ is the spacer thickness (m), ε is the porosity (–) and $conduct_{HC}$ and $conduct_{LC}$ are the conductivities of high and low concentration streams respectively (S·m^{-1}). Therefore, the electrical resistance of both HC and LC compartments is reduced as the spacer is thinner, and higher values of gross power density are obtained as a result [20]. These results demonstrate the relevance of the spacers thickness on the RED performance for the recovery of SGP and highlight the need for optimization for a successful deployment of the technology and consequently for its integration in water reclamation processes.

3.2. *Influence of the membranes thickness*

The influence of the membrane thickness is studied in this section employing both types of spacers, 20 membrane pairs and flowing both streams at 2.5 cm·s^{-1} as linear velocity. As previously explained, membranes are crucial components in the RED stack and limit the performance in the recovery of SGP. The critical properties of the ion exchange membranes include the electrical membrane resistance, the permselectivity, and the ion exchange capacity. Preceding works highlighted the importance of the commercial availability of IEMs specifically designed for RED applications with enhanced physical and electrochemical characteristics that increase energy efficiency and enable the wider deployment of the technology [54]. In this sense, Fig. 3 depicts the results accomplished, indicating the better performance obtained when using 50 μm membranes regardless of the spacer selected. Results with membranes of 50 μm thickness and 20 membrane pairs showed maximum gross power densities of 1.59 and 1.77 W·m^{-2} using spacers of 270 μm and 155 μm, respectively. Besides, the limiting current presented the same trend. When membranes of 30 μm thickness were employed (using spacers of 155 μm), 0.9 A was the maximum current value obtained; however, using membranes of 50 μm (spacers of 155 μm) the limiting current increased up to 1.1 A. After the comparative analysis of the results achieved with different membranes and the results with spacers of different thickness, it is possible to conclude the stronger influence of the membrane thickness over the thickness of the spacer, at least in the range of values studied in this work.

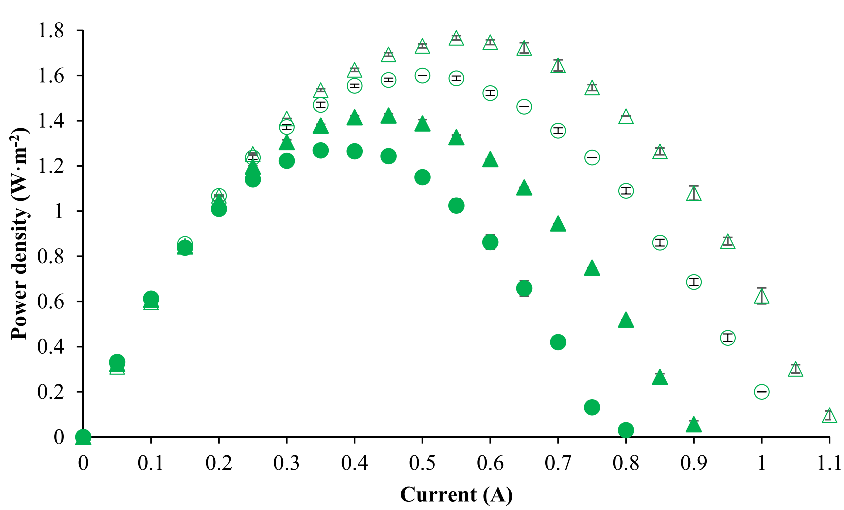

Fig. 3. Membrane thickness influence. Linear velocity = 2.5 cm·s^{-1}. ● = 270 μm spacers and ▲ = 155 μm spacers. ▲ = 30 μm membrane thickness. △ = 50 μm membrane thickness.

In reverse electrodialysis (RED), ultra-thin membranes have been widely studied in recent years since the SGP yield increases as the membrane thickness is reduced, especially below 100 μm. However, according to the results reported in this work and in accordance with previous works, IEMs with thickness lower than 40–50 μm may lead to a loss of performance and a consequent reduction in the power density [55]. Two main factors can cause this reduction in the voltage. First, in terms of the membrane characteristics, the thinnest membranes have lower values of permselectivity, as shown in Table 1. On the other hand, another critical factor which has an outstanding influence on the membrane performance is the water flux through the membranes. The water that crosses the membrane rises as the thickness decreases according to Eq. 3 [17].

$$J_{H_2O} = \frac{2\cdot D_{H_2O}}{\delta_m}\cdot\left(\left(C_{HC}^{Na^+} + C_{HC}^{Cl^-}\right) - \left(C_{LC}^{Na^+} + C_{LC}^{Cl^-}\right)\right) \quad (3)$$

where J_{H2O} ($mol\cdot m^{-2}\bullet s^{-1}$) is the osmotic flux of water, δm (m) is the membrane thickness and D_{H2O} ($m^2\cdot s^{-1}$) is the water diffusivity.

In this sense, Tedesco et al. (2018) discussed the effect of the increment in the water flux on the efficiency of the ions transport through the membrane leading to losses in the voltage output of the stack. Although these authors established that this water flux affects membranes with less than 20 μm thickness, in this study, the results show that membranes of 30 μm thickness are probably also affected by this phenomenon [56].

Consequently, from the experimental results and the literature information [55–57], the optimal range for the membrane thickness is relevant to the stack performance. IEMs must be thicker than, at least, 30 μm to avoid the different phenomena that cause power efficiency losses, and not thicker than 60–80 μm due to the upsurge in the electrical resistance.

3.3. Influence of the number of cell pairs in RED performance

Normalization of power into power density is very convenient to analyze the technology performance regardless of the number of cell pairs installed. However, the results obtained working with 3, 5, 10, 15, and 20 membrane pairs suggest that the RED technology requires, at least, a specific membrane area to reach the optimal power density.

Fig. 4 depicts the behavior when different membrane pairs are assembled employing spacers and membranes with a thickness of 270 μm and 50 μm, respectively. Ideally, the graphed curves must overlap, but this figure points to the RED underperformance when 3, 5, and 10 membranes pairs are used. Otherwise, when 15 and 20 membrane pairs are assembled, the experimental results are concordant, and therefore polarization and power curves are similar.

To visualize the impact of membrane pairs, Fig. 5 illustrates the maximum gross power density obtained and its deviation when 3 to 20 cell pairs were assembled using 270 μm spacers with membranes of 50 μm thickness (case study a) and 155 μm spacers with 30 μm membrane thickness (case study b). As it was previously mentioned, the optimal gross power density is obtained when at least 15 membrane pairs are assembled. To clarify this point, when only three pairs are inserted, the maximum gross power density was 0.4 $W\cdot m^{-2}$ and 0.7 $W\cdot m^{-2}$ for the case studies a and b, respectively. However, when 20 (or 15), membrane pairs are placed the gross power density increases up to 1.4 $W\cdot m^{-2}$ (a) and 1.6 $W\cdot m^{-2}$ (b), which implies an increment of more than 70% and 56% in gross power with respect to operation with 3 membrane pairs, respectively. In addition, in both cases, the system can be considered stable since the deviations between experiments are practically negligible. This effect is probably intrinsically related to the electrode resistance and therefore this contribution could be considered negligible when at least 15 membrane pairs were assembled, since the gross power remains constant as more membrane pairs are installed. Also, this value is in good agreement with previous literature data when seawater and 0.02 M NaCl solution were used as high and low concentration solutions, respectively.

Previous works highlighted the necessity of installing at least 50 membrane pairs to neglect the electrode resistance when reversal electrodialysis is applied. Still, in some cases, this is due to the effective membrane area since the RED module is too small and therefore parasitic currents may appear [58]. However, introducing a higher number of cell pairs could result in a reduction of the power density due to the distance to the electrodes. To avoid this disadvantage, recent works point to electrode segmentation as a new strategy [59,60].

3.4. Influence of the linear velocity of aqueous streams in the RED stack

The linear velocity of the streams flowing through the RED module is intimately linked to the gross power density [53], and therefore, a specific working range is widely recommended. In this work, the RED supplier company suggests working between 1 and 3 $cm\cdot s^{-1}$. In this sense, different experiments were developed using both the spacers and the membranes previously studied with 20 membrane pairs assembled. Fig. 6 shows the maximum gross power density achieved for the different linear velocities analyzed. When 50 μm thickness membranes were used, the power density was kept almost constant around 1.75 $W\cdot m^{-2}$. Although the theoretical gross power density increases as the linear velocity rises, previous works pointed out that the power density

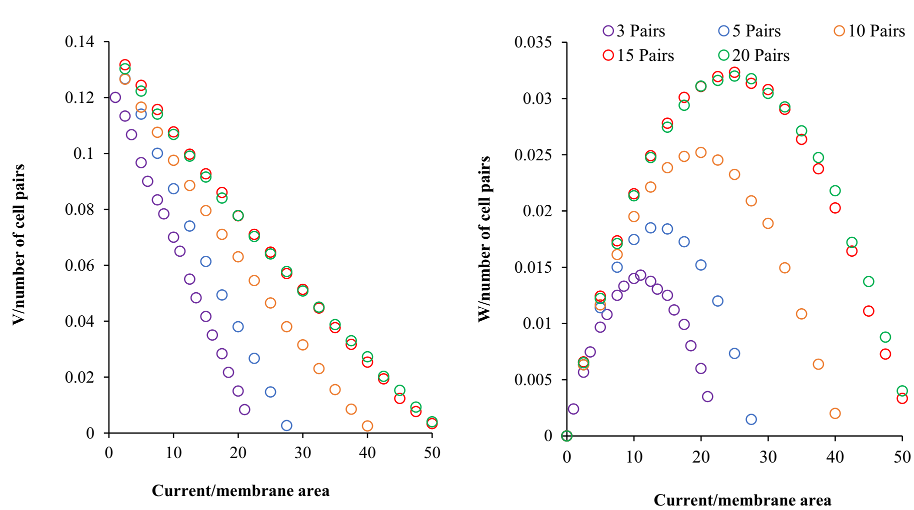

Fig. 4. Polarization and power curves. Membrane thickness = 50 μm, spacer thickness = 270 μm spacers. Linear velocity = 2.5 $cm\cdot s^{-1}$.

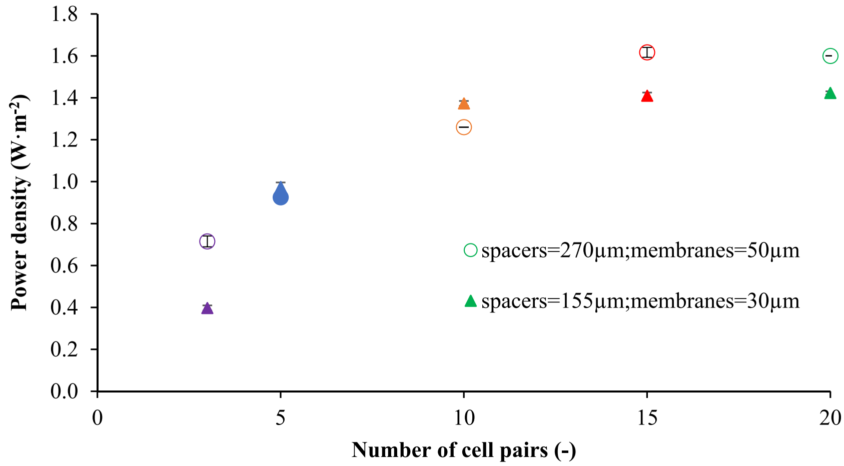

Fig. 5. Membrane pair influence in SGP performance using RED technology when two thickness spacers are employed. Membrane thickness = 50 μm. Linear velocity = 2.5 cm·s^{-1}. ○ = 270 μm spacers. △ = 155 μm spacers. (For interpretation of the references to colour in this figure legend, the reader is referred to the web version of this article.)

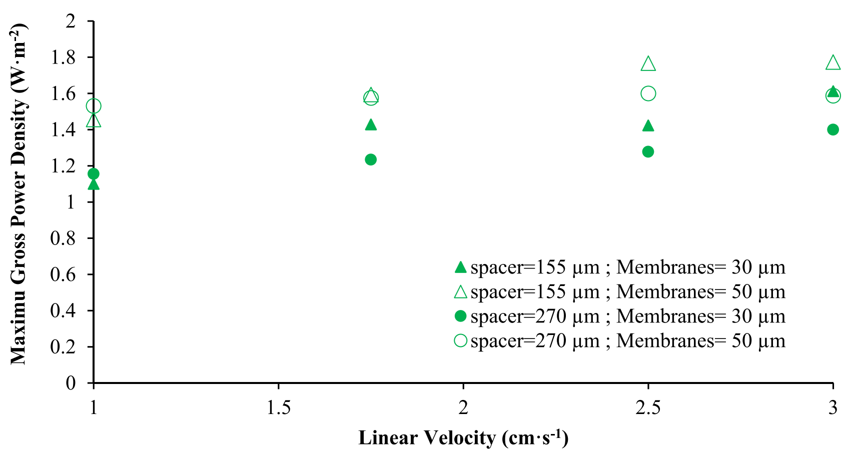

Fig. 6. Linear velocity influence on SGP performance using RED technology. ● = 270 μm spacers and ▲ = 155 μm spacers. ▲ = 30 μm membrane thickness. △ = 50 μm membrane thickness. (For interpretation of the references to color in this figure legend, the reader is referred to the web version of this article.)

increased until a plateau was reached, probably counterbalanced by the pressure drop since the red stack is close to its maximum operational velocity [45,61,62].

On the contrary, the results employing membranes of 30 μm thickness do not achieve constant values and increase as the fluids velocity increases. This fact implies that the thinnest membranes reduce the membrane resistance as expected. Consequently, the highest linear velocity is more beneficial in terms of gross power density because the higher water flux does not translate into a significant pressure drop. In addition, 50 μm membranes showed minor variations for different flow rates while the increment in the linear velocity from 1 cm·s^{-1} to 3 cm·s^{-1} translated into an increment close to 20% when 30 μm membranes were studied.

4. Conclusions

This paper contributes to a better understanding of the performance of RED technology in terms of the influence of the main components of the membrane stack, i.e., spacers thickness, ion exchange membranes thickness, the number of cell pairs assembled, and linear velocity of the flowing streams through the module in the recovery of SGE. The influence of these factors is relevant to the broader deployment of the technology in scenarios like coastal wastewater treatment plants where energy recovery can be integrated with the process of water reclamation. This work demonstrates the more decisive influence of membranes thickness over spacers thickness. Employing 20 membrane pairs, the use of 30 μm, and 50 μm thickness of membranes increases the power density from 1.28 W·m^{-2} to 1.60 W·m^{-2} using 270 μm spacers due to the fact that the thinnest membranes promote higher water flux with a lower permselectivity. On the other hand, working with 30 μm membranes, the results achieve 1.42 W·m^{-2} for 270 μm of spacers thickness. The influence of the number of cell pairs establishes that to reach the maximum gross power density of 1.77 W·m^{-2} using 155 μm spacers, at least 15 membrane pairs must be assembled; this value of gross power density is one of the best values reported in the recent literature so far when 0.5 M, typical NaCl seawater concentration and 0.02 M were used as HC and LC, respectively. Thus, future efforts addressing the reduction of the spacer thickness, employing 50 μm thickness membranes, and improving the geometry of RED modules to maximize the power density should be performed.

Declaration of competing interest

The authors declare that they have no known competing financial interests or personal relationships that could have appeared to influence the work reported in this paper.

Acknowledgments

This research has been funded by the LIFE programme (LIFE19 ENV/ES/000143) and the Spanish Ministry of Science and Innovation (RTI2018-093310-B-I00, PDC2021-120786-I00 and PLEC2021-007718). Besides, this research is also being supported by the Project "HYLANTIC" — EAPA_204/2016, which is co-financed by the European Regional Development Fund in the frame-work of the Interreg Atlantic program.

References

[1] United Nations, The 17 goals | Sustainable Development, Sustainable Development (2016). https://sdgs.un.org/goals. (Accessed 20 January 2022).
[2] J. Veerman, M. Saakes, S.J. Metz, G.J. Harmsen, Reverse electrodialysis: performance of a stack with 50 cells on the mixing of sea and river water, J. Membr. Sci. 327 (2009) 136–144, https://doi.org/10.1016/j.memsci.2008.11.015.
[3] M. AzadiAghdam, A. Achilli, S.A. Snyder, J. Farrell, Increasing water recovery during reclamation of treated municipal wastewater using bipolar membrane electrodialysis and fluidized bed crystallization, J. Water Process Eng. 38 (2020), 101555, https://doi.org/10.1016/j.jwpe.2020.101555.
[4] M. Vanoppen, T. van Vooren, L. Gutierrez, M. Roman, L.J.P. Croué, K. Verbeken, J. Philips, A.R.D. Verliefde, Secondary treated domestic wastewater in reverse electrodialysis: what is the best pre-treatment? Sep. Purif. Technol. 218 (2019) 25–42, https://doi.org/10.1016/j.seppur.2018.12.057.
[5] L. Gómez-Coma, V.M. Ortiz-Martínez, M. Fallanza, A. Ortiz, R. Ibañez, I. Ortiz, Blue energy for sustainable water reclamation in WWTPs, J. Water Process Eng. 33 (2020), 101020, https://doi.org/10.1016/j.jwpe.2019.101020.
[6] H. Manzoor, M.A. Selam, F.Bin Abdur Rahman, S. Adham, M. Castier, A. Abdel-Wahab, A tool for assessing the scalability of pressure-retarded osmosis (PRO) membranes, Renewable Energy 149 (2020) 987–999, https://doi.org/10.1016/j.renene.2019.10.098.
[7] B.E. Logan, M. Elimelech, Membrane-based processes for sustainable power generation using water, Nature 488 (2012) 313–319, https://doi.org/10.1038/nature11477.
[8] E. Farrell, M.I. Hassan, R.A. Tufa, A. Tuomiranta, A.H. Avci, A. Politano, E. Curcio, H.A. Arafat, Reverse electrodialysis powered greenhouse concept for water- and energy-self-sufficient agriculture, Appl. Energy 187 (2017) 390–409, https://doi.org/10.1016/j.apenergy.2016.11.069.
[9] E. Fontananova, E. Curcio, G. Di Profio, A.H. Avci, R.A. Tufa, Reverse electrodialysis for energy production from natural river water and seawater, Energy 165 (2018) 512–521, https://doi.org/10.1016/j.energy.2018.09.111.
[10] E. Curcio, G.Di Profio, E. Fontananova, E. Drioli, Membrane technologies for seawater desalination and brackish water treatment, in: Advances in Membrane Technologies for Water Treatment, 2015, pp. 412–440, https://doi.org/10.1016/B978-1-78242-121-4.00013-7.
[11] M. Tedesco, E. Brauns, A. Cipollina, G. Micale, P. Modica, G. Russo, J. Helsen, Reverse electrodialysis with saline waters and concentrated brines: a laboratory investigation towards technology scale-up, J. Membr. Sci. 492 (2015) 9–20, https://doi.org/10.1016/j.memsci.2015.05.020.
[12] J. Kim, J. Lee, J.H. Kim, Overview of pressure-retarded osmosis (PRO) process and hybrid application to sea water reverse osmosis process, Desalin. Water Treat. 43 (2012) 193–200, https://doi.org/10.1080/19443994.2012.672170.
[13] W.Y. Chia, S.R. Chia, K.S. Khoo, K.W. Chew, P.L. Show, Sustainable membrane technology for resource recovery from wastewater: forward osmosis and pressure retarded osmosis, J. Water Process Eng. 39 (2021), 101758, https://doi.org/10.1016/j.jwpe.2020.101758.
[14] J. Choi, Y. Oh, S. Chae, S. Hong, Membrane capacitive deionization-reverse electrodialysis hybrid system for improving energy efficiency of reverse osmosis seawater desalination, Desalination 462 (2019) 19–28, https://doi.org/10.1016/j.desal.2019.04.003.
[15] S. Loeb, Method and apparatus for generating power utilizing pressure-retarded osmosis, 1979. No. US 4193267.
[16] R. Pattle, Production of electric power by mixing fresh and salt water in the hydroelectric pile, Nature 174 (1954), https://doi.org/10.1038/174660a0.
[17] R. Ortiz-imedio, L. Gomez-coma, M. Fallanza, A. Ortiz, R. Ibañez, I. Ortiz, Comparative performance of salinity gradient power-reverse electrodialysis under different operating conditions, Desalination 457 (2019) 8–21, https://doi.org/10.1016/j.desal.2019.01.005.
[18] M. Tedesco, A. Cipollina, A. Tamburini, G. Micale, Towards 1 kW power production in a reverse electrodialysis pilot plant with saline waters and concentrated brines, J. Membr. Sci. 522 (2017) 226–236, https://doi.org/10.1016/j.memsci.2016.09.015.
[19] L. Gómez-Coma, V.M. Ortiz-Martínez, J. Carmona, L. Palacio, P. Prádanos, M. Fallanza, A. Ortiz, R. Ibañez, I. Ortiz, Modeling the influence of divalent ions on membrane resistance and electric power in reverse electrodialysis, J. Membr. Sci. 592 (2019), 117385, https://doi.org/10.1016/j.memsci.2019.117385.
[20] D.A. Vermaas, M. Saakes, K. Nijmeijer, Doubled power density from salinity gradients at reduced intermembrane distance, Environ. Sci. Technol. 45 (2011) 7089–7095, https://doi.org/10.1021/es2012758.
[21] D.A. Vermaas, J. Veerman, M. Saakes, K. Nijmeijer, Influence of multivalent ions on renewable energy generation in reverse electrodialysis, Energy Environ. Sci. 7 (2014) 1434–1445, https://doi.org/10.1039/C3EE43501F.
[22] A.H. Avci, P. Sarkar, R.A. Tufa, D. Messana, P. Argurio, E. Fontananova, G. di Profio, E. Curcio, Effect of Mg2+ions on energy generation by reverse electrodialysis, J. Membr. Sci. 520 (2016) 499–506, https://doi.org/10.1016/j.memsci.2016.08.007.
[23] E. Guler, Y. Zhang, M. Saakes, K. Nijmeijer, Tailor-made anion-exchange membranes for salinity gradient power generation using reverse electrodialysis, ChemSusChem. 5 (2012) 2262–2270, https://doi.org/10.1002/cssc.201200298.
[24] E. Güler, W. van Baak, M. Saakes, K. Nijmeijer, Monovalent-ion-selective membranes for reverse electrodialysis, J. Membr. Sci. 455 (2014) 254–270, https://doi.org/10.1016/j.memsci.2013.12.054.
[25] A.T. Besha, M.T. Tsehaye, D. Aili, W. Zhang, R.A. Tufa, Design of monovalent ion selective membranes for reducing the impacts of multivalent ions in reverse electrodialysis, Membranes 10 (2020) 1–7, https://doi.org/10.3390/membranes10010007.
[26] J. Moreno, V. Díez, M. Saakes, K. Nijmeijer, Mitigation of the effects of multivalent ion transport in reverse electrodialysis, J. Membr. Sci. 550 (2018) 155–162, https://doi.org/10.1016/j.memsci.2017.12.069.
[27] F. Kotoka, I. Merino-Garcia, S. Velizarov, Surface modifications of anion exchange membranes for an improved reverse electrodialysis process performance: a review, Membranes 10 (2020) 160, https://doi.org/10.3390/membranes10080160.
[28] Z. Guo, Z. Ji, Y.-G. Zhang, F.-J. Yang, J. Liu, Y.-Y. Zhao, J.-S. Yuan, Effect of ions (K+, Mg2+, Ca2+ and SO42-) and temperature on energy generation performance of reverse electrodialysis stack, Electrochim. Acta 290 (2018) 282–290, https://doi.org/10.1016/j.electacta.2018.09.015.
[29] T. Rijnaarts, E. Huerta, W. van Baak, K. Nijmeijer, Effect of divalent cations on RED performance and cation exchange membrane selection to enhance power densities, Environ. Sci. Technol. 51 (2017) 13028–13035, https://doi.org/10.1021/acs.est.7b03858.
[30] L. Gómez-Coma, V.M. Ortiz-Martínez, J. Carmona, L. Palacio, P. Prádanos, M. Fallanza, A. Ortiz, R. Ibañez, I. Ortiz, Modeling the influence of divalent ions on membrane resistance and electric power in reverse electrodialysis, J. Membr. Sci. 592 (2019), 117385, https://doi.org/10.1016/j.memsci.2019.117385.
[31] A.H. Galama, N.A. Hoog, D.R. Yntema, Method for determining ion exchange membrane resistance for electrodialysis systems, Desalination 380 (2016) 1–11, https://doi.org/10.1016/j.desal.2015.11.018.
[32] J. Luque Di Salvo, A. Cosenza, A. Tamburini, G. Micale, A. Cipollina, Long-run operation of a reverse electrodialysis system fed with wastewaters, J. Environ. Manag. 217 (2018) 871–887, https://doi.org/10.1016/j.jenvman.2018.03.110.
[33] D.A. Vermaas, D. Kunteng, M. Saakes, K. Nijmeijer, Fouling in reverse electrodialysis under natural conditions, Water Res. 47 (2013) 1289–1298, https://doi.org/10.1016/j.watres.2012.11.053.
[34] D.A. Vermaas, D. Kunteng, J. Veerman, M. Saakes, K. Nijmeijer, Periodic feedwater reversal and air sparging as antifouling strategies in reverse electrodialysis, Environ. Sci. Technol. 48 (2014) 3065–3073, https://doi.org/10.1021/es4045456.
[35] K. Khoiruddin, D. Ariono, S. Subagjo, I.G. Wenten, Improved anti-organic fouling of polyvinyl chloride-based heterogeneous anion-exchange membrane modified by hydrophilic additives, J. Water Process Eng. 41 (2021), https://doi.org/10.1016/j.jwpe.2021.102007.
[36] Y. Mei, X. Li, Z. Yao, W. Qing, A.G. Fane, C.Y. Tang, Simulation of an energy self-sufficient electrodialysis desalination stack for salt removal efficiency and fresh water recovery, J. Membr. Sci. 598 (2020), 117771, https://doi.org/10.1016/j.memsci.2019.117771.
[37] D.A. Vermaas, M. Saakes, K. Nijmeijer, Enhanced mixing in the diffusive boundary layer for energy generation in reverse electrodialysis, J. Membr. Sci. 453 (2014) 312–319, https://doi.org/10.1016/j.memsci.2013.11.005.
[38] D.A. Vermaas, E. Guler, M. Saakes, K. Nijmeijer, Theoretical power density from salinity gradients using reverse electrodialysis, Energy Procedia 20 (2012) 170–184, https://doi.org/10.1016/j.egypro.2012.03.018.
[39] D.A. Vermaas, E. Guler, M. Saakes, K. Nijmeijer, Theoretical power density from salinity gradients using reverse electrodialysis, Energy Procedia 20 (2012) 170–184, https://doi.org/10.1016/j.egypro.2012.03.018.
[40] Y. Mei, C.Y. Tang, Recent developments and future perspectives of reverse electrodialysis technology: a review, Desalination 425 (2017) 156–174, https://doi.org/10.1016/j.desal.2017.10.021.
[41] A. Nazif, H. Karkhanechi, E. Saljoughi, S.M. Mousavi, H. Matsuyama, Recent progress in membrane development, affecting parameters, and applications of reverse electrodialysis: a review, J. Water Process Eng. 47 (2022), 102706, https://doi.org/10.1016/j.jwpe.2022.102706.
[42] L. Gurreri, M. Ciofalo, A. Cipollina, A. Tamburini, W. van Baak, G. Micale, CFD modelling of profiled-membrane channels for reverse electrodialysis, Desalin. Water Treat. 55 (2015) 3404–3423, https://doi.org/10.1080/19443994.2014.940651.
[43] S. Pawlowski, G. Crespo, S. Velizarov, Profiled ion exchange membranes: a comprehensible review, Int. J. Mol. Sci. 20 (2019) 165, https://doi.org/10.3390/ijms20010165.
[44] S. Mehdizadeh, M. Yasukawa, T. Abo, Y. Kakihana, M. Higa, Effect of spacer geometry on membrane and solution compartment resistances in reverse electrodialysis, J. Membr. Sci. 572 (2019) 271–280, https://doi.org/10.1016/j.memsci.2018.09.051.
[45] R. Long, B. Li, Z. Liu, W. Liu, Performance analysis of reverse electrodialysis stacks: channel geometry and flow rate optimization, Energy 158 (2018) 427–436, https://doi.org/10.1016/j.energy.2018.06.067.

[46] V. Ortiz-Martínez, L. Gomez-Coma, C. Tristán, G. Pérez, M. Fallanza, A. Ortiz, R. Ibañez, I. Ortiz, A comprehensive study on the effects of operation variables on reverse electrodialysis performance, Desalination 482 (2020), 114389, https://doi.org/10.1016/j.desal.2020.114389.
[47] J. Veerman, M. Saakes, S.J. Metz, G.J. Harmsen, Reverse electrodialysis: a validated process model for design and optimization, Chem. Eng. J. 166 (2011) 256–268, https://doi.org/10.1016/j.cej.2010.10.071.
[48] M. Micari, M. Bevacqua, A. Cipollina, A. Tamburini, W. van Baak, T. Putts, G. Micale, Effect of different aqueous solutions of pure salts and salt mixtures in reverse electrodialysis systems for closed-loop applications, J. Membr. Sci. 551 (2018) 315–325, https://doi.org/10.1016/j.memsci.2018.01.036.
[49] J. Veerman, M. Saakes, S.J. Metz, G.J. Harmsen, Reverse electrodialysis: evaluation of suitable electrode systems, J. Appl. Electrochem. 40 (2010) 1461–1474, https://doi.org/10.1007/s10800-010-0124-8.
[50] J. Veerman, D.A. Vermaas, Reverse Electrodialysis: Fundamentals, Elsevier Ltd, 2016, https://doi.org/10.1016/B978-0-08-100312-1.00004-3.
[51] M.Saakes Veerman, S.J. Metz, G.J. Harmsen, in: Electrical Power from Sea and River Water by Reverse Electrodialysis: A First Step From the Laboratory to a Real Power Plant 44, 2010, pp. 9207–9212.
[52] X. Zhu, W. He, B.E. Logan, Reducing pumping energy by using different flow rates of high and low concentration solutions in reverse electrodialysis cells, J. Membr. Sci. 486 (2015) 215–221, https://doi.org/10.1016/j.memsci.2015.03.035.
[53] R. Ortiz-Imedio, L. Gomez-Coma, M. Fallanza, A. Ortiz, R. Ibañez, I. Ortiz, Comparative performance of salinity gradient power-reverse electrodialysis under different operating conditions, Desalination 457 (2019) 8–21, https://doi.org/10.1016/j.desal.2019.01.005.
[54] J.G. Hong, H. Gao, L. Gan, X. Tong, C. Xiao, S. Liu, B. Zhang, Y. Chen, Nanocomposite and nanostructured ion-exchange membrane in salinity gradient power generation using reverse electrodialysis, in: Advanced Nanomaterials for Membrane Synthesis and Its Applications, Elsevier, 2018, pp. 295–316, https://doi.org/10.1016/B978-0-12-814503-6.00013-6.
[55] M. Tedesco, H.V.M. Hamelers, P.M. Biesheuvel, Nernst-planck transport theory for (reverse) electrodialysis: III. Optimal membrane thickness for enhanced process performance, J. Membr. Sci. 565 (2018) 480–487, https://doi.org/10.1016/j.memsci.2018.07.090.
[56] M. Tedesco, H.V.M. Hamelers, P.M. Biesheuvel, Nernst-planck transport theory for (reverse) electrodialysis: IIEffect of water transport through ion-exchange membranes, Journal of Membrane Science 531 (2017) 172–182, https://doi.org/10.1016/j.memsci.2017.02.031.
[57] M. Tedesco, H.V.M. Hamelers, P.M. Biesheuvel, Nernst-planck transport theory for (reverse) electrodialysis: IEffect of co-ion transport through the membranes, Journal of Membrane Science 510 (2016) 370–381, https://doi.org/10.1016/j.memsci.2016.03.012.
[58] A. Zoungrana, M. Çakmakci, From non-renewable energy to renewable by harvesting salinity gradient power by reverse electrodialysis: a review, Int. J. Energy Res. 45 (2021) 3495–3522, https://doi.org/10.1002/er.6062.
[59] C. Simões, D. Pintossi, M. Saakes, Z. Borneman, W. Brilman, K. Nijmeijer, Electrode segmentation in reverse electrodialysis: improved power and energy efficiency, Desalination 492 (2020), 114604, https://doi.org/10.1016/j.desal.2020.114604.
[60] H. Kim, S.C. Yang, J. Choi, J.O. Kim, N. Jeong, Optimization of the number of cell pairs to design efficient reverse electrodialysis stack, Desalination 497 (2021), 114676, https://doi.org/10.1016/j.desal.2020.114676.
[61] M. Tedesco, A. Cipollina, A. Tamburini, I.D.L. Bogle, G. Micale, A simulation tool for analysis and design of reverse electrodialysis using concentrated brines, Chem. Eng. Res. Des. 93 (2015) 441–456, https://doi.org/10.1016/j.cherd.2014.05.009.
[62] J.G. Hong, W. Zhang, J. Luo, Y. Chen, Modeling of power generation from the mixing of simulated saline and freshwater with a reverse electrodialysis system: the effect of monovalent and multivalent ions, Appl. Energy 110 (2013) 244–251, https://doi.org/10.1016/j.apenergy.2013.04.015.